IMPACT PERFORATION OF COMPOSITE SANDWICH PANELS

Michelle S. Hoo Fatt, Dushyanth Sirivolu
Department of Mechanical Engineering, The University of Akron, Akron OH 44325-3903

Keywords: Composite sandwich; impact perforation, analytical models.

Abstract

Analytical models for the quasi-static and low-velocity perforation of composite sandwich panel with woven roving E-glass/vinyl ester facesheets and Coremat™ were developed. A multi-stage perforation process involving delamination, debonding, core shear fracture and facesheet fracture was used to calculate the quasi-static failure load and ballistic limit of the panel. The high core crushing resistance of the Coremat™ caused the distal facesheet to fracture before the incident facesheet during panel perforation. This is in contrast to sandwich panel with honeycomb and conventional polymeric foams, whereby damage first occurs on the incident faceheet. Analytical predictions of the quasi-static load-deflection response and the dynamic contact force history were within 10% of the test results.

1 Introduction

Composite sandwich panels are used extensively in the aerospace, marine, transportation, and recreational industries because of their high specific stiffness and strength, corrosion resistance, tailorability, and high fatigue life. In many of these applications, the composite panel may be subjected to localized projectile impact. Therefore, much work has been done in an effort to determine the failure load, ballistic limit, perforation energy and damage induced into composite sandwich panels subjected to quasi-static indentation and projectile impact [1-3]. While most of this research has been experimental, few analytical solutions have been proposed because of the complicated interaction between the composite facesheet and core during deformation and failure.

The objective of this paper is to present analytical models that can be used to describe quasi-static and impact perforation of an E-glass/vinyl ester and Coremat™ sandwich panel. The analytical models are derived using experimental results from Mines et al. [3]. In Ref. [3], quasi-static and low-velocity impact perforation tests with a hemispherical-ended indenter/projectile were done on two types of composite sandwich panels: a woven roving E-glass/vinyl ester skin with Coremat™ core and an E-glass/epoxy with an aluminum honeycomb core. Coremat™ is a high density/high energy absorption resin impregnated non-woven polyester with 50% microsphere and is commonly used in the marine industry [4]. Although the mechanical properties of the facesheets in both sandwich panels were similar in these tests, the Coremat had a much higher crushing resistance than the aluminum honeycomb. As a result of this, failure in the Coremat sandwich first occurred on the back (distal) facesheet while failure in the aluminum honeycomb sandwich occurred on the front (incident) facesheet. In earlier work, Lin and Hoo Fatt [5] developed an analytical model to describe the quasi-static and impact perforation the E-glass/epoxy with the aluminum honeycomb core. This paper is an extension of earlier work to develop analytical models for the impact perforation of composite sandwich panels.

2 Problem Formulation

Consider the composite sandwich panel, as shown in Fig. 1. The facesheets are thin orthotropic membranes of dimension a x a x h, and the core is a crushable polymeric foam of dimension a x a x H. This particular core is made of a Coremat, which has a core crushing resistance that is linear strain-hardening [3]. Typical low-density foam cores have constant core crushing resistance. The indenter/projectile has a hemispherical-nose of radius R and a mass M_o. The indenter/projectile is assumed rigid compared to the sandwich panel.

Upon loading, the panel experiences simultaneous local indentation and global deformation. Analytical solutions for the local load-deflection as well as the global load-deflection will be derived using the principle of minimum potential energy in the following section. Experiments [1-3] indicate the fracture mechanisms as well as the load-displacement characteristics of sandwich panels subjected to low-velocity impact are similar to those observed in quasi-static cases. Three stages must occur for total perforation of the sandwich panel: (i) initial failure during which one of the skins of the panel fractures; (ii) penetration of the indenter through core and surviving facesheet; and (iii) complete panel perforation including frictional resistance between the indenter/projectile and sandwich panel. Delamination, debonding, core shear fracture, and tensile fracture of incident and distal facesheets occur during the perforation process. The order in which these failure mechanisms occur depends on geometry and material properties. Simple analytical failure criteria have been proposed for composite sandwich beam structures [6], but these cannot be directly applied to the composite sandwich plate.

3 Static Perforation

Approximate solutions for the quasi-static local indentation and global deformation of a composite sandwich panel will be derived using the principle of minimum potential energy. Local indentation consists of front facesheet indentation and core crushing, while global deformation consists of bending and shearing of the entire panel. Local indentation and global deformation will be considered independently, and the total panel deformation is considered as the sum of the local indentation and global deformation. When either the top or bottom facesheet fails, both local and global load-deflection characteristics will change. Complete sandwich panel perforation does not occur until both facesheets and core have failed.

3.1 Local indentation

Top facesheet indentation is modeled by considering a rigid indenter pressing into an orthotropic membrane resting on a rigid-plastic foundation. The total potential energy of the system is

$$\prod = U + D - W \tag{1}$$

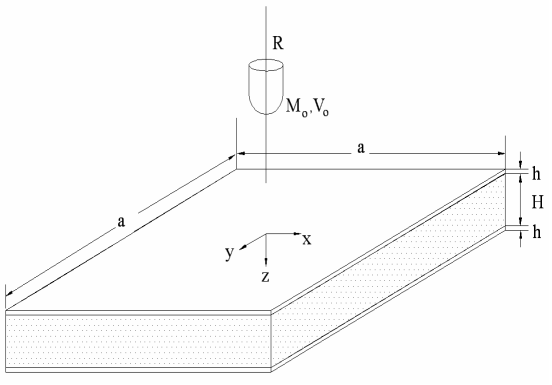

Fig. 1 Geometry of composite sandwich panel.

where *U* is the elastic strain energy of the facesheet, *D* the work dissipated in crushing the core, and *W* the external work done.

Under moderately large deflection, the facesheet responds like an orthotropic membrane. The strain energy associated with bending is negligible compared to the membrane energy associated with in-plane stretching. In addition, in-plane deformations, u and v, are negligibly small compared to transverse deflections, w. With these two assumptions, the elastic strain energy becomes

$$U = \frac{1}{8}\int_S \left[A_{11}\left(\frac{\partial w}{\partial x}\right)^4 + A_{22}\left(\frac{\partial w}{\partial y}\right)^4 + \left(2A_{12} + 4A_{66}\right)\left(\frac{\partial w}{\partial x}\right)^2\left(\frac{\partial w}{\partial y}\right)^2 \right] dS \tag{2}$$

where A_{ij} is the membrane stiffness of the orthotropic facesheet and S is the area.

The work dissipated in crushing the Coremat is given by

$$D = \int_S \left(a_1 + \frac{k}{H} w \right) w dS \tag{3}$$

where a_1 and k are the core's crushing flow strength and strain hardening modulus, respectively.

The exact solution for the transverse deflection of an axi-symmetrical isotropic plate under center point loading is used to describe the local indentation of the sandwich panel, w:

$$w(r) = \delta\left[1 - \frac{r}{\xi}\right]^2 \qquad (4)$$

where δ s the local indentation under the indenter, ξ is the length of the deformation zone, and $r^2 = x^2 + y^2$. The total potential energy then becomes

$$\prod = C_1 \frac{\delta^4}{\xi^2} + \frac{\pi a_1}{6}\delta\xi^2 + \frac{k\pi}{15H}\delta^2\xi^2 - P\delta \qquad (5)$$

where $C_1 = \frac{\pi}{60}(3A_{11} + 3A_{22} + 2A_{12} + 4A_{66})$.. The total potential energy $\prod$ is a function of two unknown parameters, ξ and δ. From the principle of minimum potential energy, an equilibrium condition occurs when $\frac{\partial \prod(\delta,\xi)}{\partial \delta} = 0$. Minimizing the potential energy yields the following load-indentation response:

$$P = \frac{4C_1\delta^3}{\xi^2} + \frac{\pi a_1 \xi^2}{6} + \frac{2\pi k\delta\xi^2}{15H} \qquad (6)$$

The load-deformation response is dependent on ξ and is minimum when $\frac{\partial P}{\partial \xi} = 0$. Therefore,

$$P = 4C_1\delta\sqrt{\frac{\left(5\pi a_1 H\delta + 4\pi k\delta^2\right)}{120C_1H}} + \left(\frac{5\pi a_1 H\delta^2 + 4\pi k\delta^3}{30H}\right)\sqrt{\frac{120C_1H}{\left(5\pi a_1 H\delta + 4k\pi\delta^2\right)}} \qquad (7)$$

The first term in the right-hand side of Eq. (7) represents membrane resistance of the facesheet, while the second term in Eq. (7) is due to the Coremat crushing resistance.

3.2 Global panel deformation

Again assuming in-plane deformations are negligible compared to the transverse deformation, one finds the following expression for the elastic strain energy of the symmetric sandwich panel with orthotropic facesheet:

$$U = 4\int_0^a\int_0^a \left\{\frac{D_{11}^s}{2}\left(\frac{\partial\bar{\alpha}}{\partial x}\right)^2 + D_{12}^s\left(\frac{\partial\bar{\beta}}{\partial y}\right)\left(\frac{\partial\bar{\alpha}}{\partial x}\right) + \frac{D_{22}^s}{2}\left(\frac{\partial\bar{\beta}}{\partial y}\right)^2 + A_{55}^s\left[\frac{\bar{\alpha}^2}{2} + \bar{\alpha}\frac{\partial w}{\partial x} + \frac{1}{2}\left(\frac{\partial w}{\partial x}\right)^2\right] + A_{44}^s\left[\frac{\bar{\beta}^2}{2} + \bar{\beta}\frac{\partial w}{\partial y} + \frac{1}{2}\left(\frac{\partial w}{\partial y}\right)^2\right] + D_{66}^s\left[\frac{1}{2}\left(\frac{\partial\bar{\alpha}}{\partial y}\right)^2 + \frac{\partial\bar{\alpha}}{\partial y}\frac{\partial\bar{\beta}}{\partial x} + \frac{1}{2}\left(\frac{\partial\bar{\beta}}{\partial x}\right)^2\right]\right\} dxdy \qquad (8)$$

where w is again used to express transverse deflections, $\bar{\alpha}$ and $\bar{\beta}$ are shear angles associated with the x- and y-directions, respectively, D_{ij}^s is the sandwich bending stiffness matrix, and A_{44}^s and A_{55}^s are the transverse shear stiffnesses. The superscript "s" is used to denote the sandwich.

Finite element analysis using ABAQUS Standard was used to describe the transverse deformation, w, and the shear rotations with respect to the x- and y-axis, $\bar{\alpha}$ and $\bar{\beta}$, as follows:

$$w(x,y) = \Delta\left(1 - \left(\frac{x}{a}\right)^2\right)^2\left(1 - \left(\frac{y}{a}\right)^2\right)^2 \qquad (9)$$

and

$$\bar{\alpha}(x,y) = \alpha_o \sin\left(\frac{\pi x}{a}\right)\left(1 - \left(\frac{y}{a}\right)^2\right)^2 \qquad (10)$$

$$\bar{\beta}(x,y) = \beta_o \sin\left(\frac{\pi y}{a}\right)\left(1 - \left(\frac{x}{a}\right)^2\right)^2 \qquad (11)$$

where Δ is the global deflection under the indenter and α_o and β_o are rotations at the center of the panel. The above functions satisfy the boundary conditions that $w = 0$ and $\bar{\alpha} = \bar{\beta} = 0$ at the edges.

Substituting derivatives of the expressions in Eqs. (9)-(11) into Eq. (8) gives the following expression for the strain energy:

$$U = F_1\Delta^2 + F_2\alpha_o^2 + F_3\beta_0^2 + F_4\Delta\alpha_0 + F_5\Delta\beta_0 + F_6\alpha_0\beta_0 \qquad (12)$$

where

$$F_1 = \frac{32768}{33075}\left(A^s_{44} + A^s_{55}\right)$$

$$F_2 = \frac{128}{315}a^2 A^s_{55} + \frac{128\pi^2}{315}D^s_{11} + \frac{128}{105}D^s_{66}$$

$$F_3 = \frac{128}{315}a^2 A^s_{44} + \frac{128\pi^2}{315}D^s_{22} + \frac{128}{105}D^s_{66}$$

$$F_4 = \frac{-4096}{105\pi^3}aA^s_{55}$$

$$F_5 = \frac{-4096}{105\pi^3}aA^s_{44}$$

$$F_6 = \frac{2304}{\pi^6}\left(D^s_{12} + D^s_{66}\right)$$

The total potential energy then becomes

$$\Pi = F_1\Delta^2 + F_2\alpha_o^2 + F_3\beta_0^2 + F_4\Delta\alpha_0 + F_5\Delta\beta_0 + F_6\alpha_0\beta_0 - P\Delta \qquad (13)$$

Minimizing Π with respect to Δ, α_o and β_o gives a closed-form expression for the global load-deflection response,

$$P = K_g\Delta \qquad (14)$$

where $K_g = \dfrac{\left|4F_1(F_2 + F_3 + F_6) - (F_4 + F_5)^2\right|}{2(F_2 + F_3 + F_6)}$.

Table 1 gives the facesheet and core material properties for the sandwich panels considered in this research. Most of these material properties come from Ref. [3], but some have been estimated from Refs. [7] and [8]. These material properties were used to calculate the local indentation and global deformation under static indentation with a 25 mm diameter tup. A comparison of the predicted load-deflection characteristics under the tup with test data is shown from points A-C in Fig. 2. The total deflection X_1 in Fig. 2 is the displacement of the indenter. It is the sum of local indentation δ and global deformation Δ, i.e., $X_1 = \delta + \Delta$. Neither the front (incident) nor the back (distal) facesheet were perforated during this event, and the analytical solution for the load-deflection is within 5% of the test data.

Table1. Material properties of woven roving E-glass/vinyl ester and Coremat.

	E-Glass/ Vinyl Ester	Firet Coremat
Density (kg/m^3)	1391.3	640
Thickness (mm)	0.48	9.34
E_{11} (+) (GPa)	17	0.8
E_{22} (+) (GPa)	17	0.8
E_{33} (GPa)	--	0.35
ν_{12}	0.13	0.36
ν_{13}	--	0.57
ν_{23}	--	0.57
ν_{21}	0.13	0.36
ν_{31}	--	0.45
ν_{32}	--	0.45
G_{12}=G_{21} (GPa)	4.0	0.29
G_{23}=G_{32} (GPa)	--	0.068
G_{13}=G_{31} (GPa)	--	0.068
σ_{3f} (-) (MPa)	--	22
a_1 (MPa)	--	10
k (MPa)	--	100
ILSS (MPa)	51.6	51.6*
G_{IIC} (J/m^2)	2757	1400
σ_{1f} (+) (MPa)	270	--
σ_{1f} (-) (MPa)	200	--
σ_{2f} (+) (MPa)	270	--
σ_{2f} (-) (MPa)	200	--
τ_{12f} (+)=τ_{21f} (+) (MPa)	40	--
τ_{13f} (+)=τ_{31f} (+) (MPa)	--	5
τ_{23f} (+)=τ_{32f} (+) (MPa)	--	5
ε_{1f} (+)	0.021	--
ε_{3f} (-)	--	0.025
E_a (MJ/m^3)	2.7	--

* Interlaminar shear strength is assumed equal to E-Glass/vinyl ester.

4 Failure Mechanisms

As mentioned earlier several failure mechanisms may occur during local indentation and global deformation. Simple failure criteria are derived for each of these mechanisms below. A multi-stage damage model to complete perforation will be proposed once the initial failure mechanism is determined.

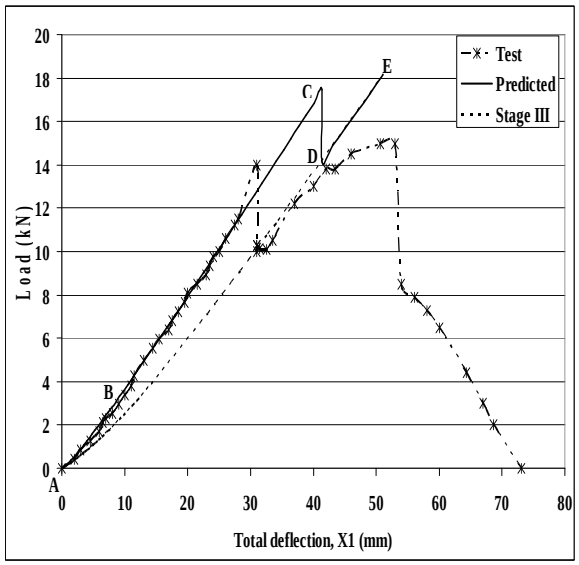

Fig. 2 Variation of quasi-static load with penetrator displacement.

4.1 Delamination/debonding

Although not a catastrophic failure mode, delamination between plies and debonding between facesheets and core will occur when the interlaminar shear strength and bond strength are exceeded. Fracture mechanics can be used to calculate threshold loads for the onset of delamination and debonding. An approximate solution for the delamination threshold load in a quasi-isotropic orthotropic plate under static indentation is given by Olsson et al. [9] as

$$P_{del}^{st} = \pi\sqrt{\frac{32G_{IIc}D}{3}} \qquad (15)$$

where G_{IIc} is the Mode II interlaminar fracture toughness and $D = \sqrt{D_{11}D_{22}(\eta+1)/2}$, $\eta = (D_{12}+2D_{66})/\sqrt{D_{11}D_{22}}$. This formula can be used to calculate the threshold load for delamination/debonding in the E-glass/vinyl ester and Coremat sandwich panel by assuming $D_{ij} = D_{ij}^{s}$. Under impact loads, the threshold delamination load is $P_{del}^{dyn} = 1.213P_{del}^{st}$. Separate loads should be calculated for delamination and debonding because values for the Mode II interlaminar shear fracture toughness are generally not the same.

The size of the delamination may found from equilibrium considerations and assuming that the transverse stress is parabolic through the thickness,

$$\tau_{rz} = \frac{3P}{4\pi r(H+2h)}\left[1-\left(\frac{2z}{H+2h}\right)^2\right] \qquad (16)$$

where r and z are the radial and through-thickness coordinates, respectively. The delamination or debonding radius is found by evaluating τ_{rz} at the appropriate interlayer and stetting it equal to the interlaminar shear strength of the facesheet or the interlaminar bond strength of between the facesheet and core.

4.2 Core shear failure

Consider local indentation of isolated Coremat (no facesheet) by the hemispherical-nose indenter. The crushing load under the indenter is given by

$$P = 2\pi\int_0^{\rho}\left(a_1+\frac{kw}{H}\right)rdr \qquad (17)$$

where $w = \sqrt{R^2-r^2}+\delta-R$ is the local deflection under the indenter and ρ is the contact radius of the indenter with the top facesheet. A simple relation between local indentation δ and contact radius ρ is given by

$$\delta = R-\sqrt{R^2-\rho^2} \qquad (18)$$

Isolated core shear failure takes place when $P = P_c = 2\pi\rho_c H\tau_{cr}$, where ρ_c is the critical contact radius at core shear failure and $\tau_{cr} = \tau_{13}$ is the transverse shear strength of Coremat. Integrating Eq. (17), using Eq. (18) to eliminate δ, and setting $P = P_c$ give the following implicit solution for ρ_c:

$$\frac{a_1\rho_c}{2H}+\frac{k}{3\rho_c H^2}\left[R^3-\left(R^2-\rho_c^2\right)^{\frac{3}{2}}\right] - \frac{k\rho_c}{2H^2}\sqrt{R^2-\rho_c^2} = \tau_{cr} \qquad (19)$$

The corresponding load for isolated core shear fracture can be calculated once ρ_c is known. The load at which the Coremat sandwich panel undergoes core shear failure is higher than the core shear fracture load of isolated Coremat since the sandwich also has to resist the front facesheet membrane resistance. The core shear fracture load for the Coremat sandwich panel is found by requiring the second term of Eq. (7) be equal to P_c.

4.3 Front/back facesheet failure

One can use strain energy density to predict facesheet failure. The strain energy density in an orthotropic facesheet is

$$U_o = \frac{1}{2}(\overline{Q}_{11}\varepsilon_x^2 + \overline{Q}_{22}\varepsilon_y^2 + 2\overline{Q}_{12}\varepsilon_x\varepsilon_y + \overline{Q}_{66}\gamma_{xy}^2) \quad (20)$$

where ε_x, ε_y, and γ_{xy} are in-plane strains and $\overline{Q}_{ij}$ are components of the transformed stiffness matrix. When the strain energy density is larger than the toughness, i.e, the specific energy absorbed in a uniaxial tension test E_a, failure can occur.

In the back facesheet, the strain varies through the sandwich panel thickness and are given by

$$\varepsilon_x = z\frac{\partial\overline{\alpha}}{\partial x}, \varepsilon_y = z\frac{\partial\overline{\beta}}{\partial y}, \quad \text{and} \quad \gamma_{xy} = z\left(\frac{\partial\overline{\alpha}}{\partial x} + \frac{\partial\overline{\beta}}{\partial y}\right).$$

where Eqs. (10) and (11) are used to evaluate strains. According to these expressions, the maximum compressive and tensile strains due to global deformation occur in the front and back facesheets, respectively. The front facesheet strains may be estimated by the average strain method presented in Ref. [5]. Since the strains due to local indentation in the front facesheet are tensile and opposite in sign to the compressive strains caused by global bending, the magnitude of the strains in the back facesheet is always larger. Failure due to global deformation will therefore first occur in the back facesheet rather than the front facesheet.

Our calculated results show that the strain energy density in both front and back facesheets are maximum under the indenter and along the 0 and 90° directions. This means cracks in the front or back facesheet will emanate in four directions corresponding to the 0 and 90° reinforcement directions of the woven skins.

The failure loads for delamination, debonding, cores shear fracture, and back facesheet fracture are given in Table 2. The lowest load corresponds to core shear fracture, thereby signifying that this takes place before fracture of either top or bottom facesheets. Since the core is still trapped between facesheets, the local indentation and global deformation response remain relatively unchanged. After core shear fracture, the contact radius between indenter and top facesheet still increases with load and the Coremat crushes with almost the same characteristics as when there was no core shear fracture. Debonding and delamination then takes place at 7.6 and 10.7 kN, respectively. The back facesheet finally fractures at 17.4 kN. This is about 25% higher than the experimental failure load at 14 kN. Approximate energy methods are generally less accurate in predicting stresses and strains than they are deflections.

When the back facesheet fails, new load-deflection relations must be derived since the panel becomes weaker and less stiff. A progressive or multi-stage perforation model will be used to derive these new load-deflection relations in the next section.

Table 2. Load and deflection at each failure mode.

Failure Mode	Load (kN)	Local Indentation (mm)	Global Deflection (mm)
Delamination	10.7	4.5	23.8
Debonding	7.6	3.8	17.4
Core Shear	3.8	2.6	8.6
Back Facesheet	17.4	5.9	36.8

4.4 Multi-stage perforation model

The following multi-stage perforation model is proposed as illustrated in Figure 3 (a)-(c):

Stage I – Local indentation and global deformation up to core shear fracture, as depicted in Fig. 3 (a). Core shear fracture occurs at roughly 45 degrees with respect to the plane of the panel since this corresponds to a plane of maximum shear stress. It is easier for the crack to extend horizontally thereby debonding the core from the back facesheet rather than continue at the 45 degree angle into the facesheet. The transverse bond strength is an order of magnitude smaller than the transverse shear strength of the facesheet.

Stage II – Deformation beyond core shear fracture and ending with back facesheet fracture, as indicated in Fig. 3 (b). The core crushing resistance used to calculate the local load-indentation response remains unchanged since the facesheet are intact. Eventually a cross-hair fracture develops on the back facesheet, as is also shown in Fig. 3(b).

Stage II I– Deformation up to front facesheet fracture (see Fig. 3 (c)). Both global and local deformation continues after the back facesheet fails. The back facesheet petals under the indenter and local indentation becomes softer. A new load-deformation response will occur in Stage III and will be discussed in the next section. The global panel stiffness is little affected by the cross-hair fracture and is assumed to be roughly the same prior to back facesheet fracture.

4.4 Back facesheet debonding after core shear fracture

Back facesheet debonding is triggered by core shear fracture at a 45 degree angle. The size (radius) of the back facesheet debond λ can be calculated by assuming the tensile strength at the interface of the E glass/vinylester and Coremat is $\sigma_t = 73$ [10] and the following equilibrium condition:

$$\sigma_t \pi\left(\lambda^2 - d^2\right) = \pi a_1 \rho^2 + \frac{2\pi k}{3H}\left[R^3 - \left(R^2 - \rho^2\right)^{\frac{3}{2}}\right] - \frac{\pi k \rho^2}{H}\sqrt{R^2 - \rho^2} \quad (21)$$

where $d = \rho_c + H$ is the radial distance to the start of the debonding region and ρ_c is the critical contact radius at core shear fracture. The right-hand side of Eq. (21) is the force exerted on the back facesheet by the Coremat in terms of ρ. Since ρ is related to δ by Eq. (18), one can determine the debond radius for any load using the load-indentation relation in Eq. (7). Substituting geometric and materials properties into Eq. (19) gives $\rho_c = 7.8$ mm. Solving Eq. (21) at the back facesheet failure load and deflection gives $\lambda = 32.9$ mm.

4.5 Local indentation response in Stage III

Local petaling occurs immediately following cross-hair fracture in the back facesheet. The global sandwich panel stiffness is little affected by the localized petaling, but the local indentation resistance is much reduced, especially under the indenter. As shown in Fig. 3 (c), transverse shearing rather than compression of the Coremat is occurring beneath the indenter. Once again the minimum potential energy is used to predict the local-indentation response.

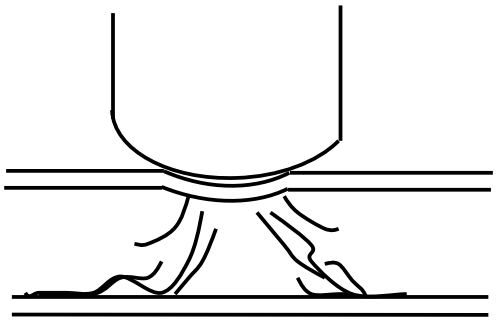

(a) Core shear fracture and back facesheet debonding.

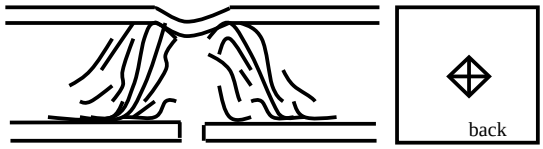

(b) Back facesheet failure.

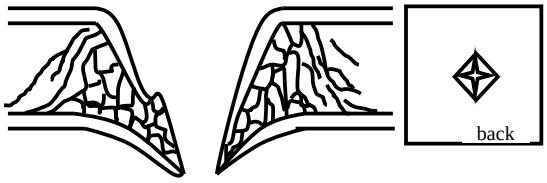

(c) Front facesheet failure and perforation.

Fig. 3 Multi-stage perforation process: (a) core shear failure and back facesheet debonding, (b) back facesheet fracture, (c) front facesheet failure and perforation.

The total potential energy during Stage III local indentation is given by

$$\Pi = C_1 \frac{\delta^4}{\lambda^2} + \frac{G_{13}\pi H}{12}\delta^2 + \frac{8\tilde{D}_{11}}{3\lambda^2}\left(\delta - \delta_c\right)^2 - P\delta \quad (22)$$

where G_{13} is the core transverse shear stiffness, $\tilde{D}_{11} = \sum_{j=1}^{N} \sqrt{E_{11_j}^2 + E_{22_j}^2}\left(z_j^3 - z_{j-1}^3\right)$ is a beam equivalent bending stiffness, N is the number of plies in the facesheet, and δ_c is the local deflection at back facesheet failure. The first term of the potential energy is the membrane energy of the front facesheet, the second term is the core shearing energy and the last term is the bending energy of four petals (see Fig. 3 (c)). Minimizing the potential energy yields the following load-indentation response:

$$P = \frac{4C_1}{\lambda^2}\delta^3 + \frac{G_{13}\pi H}{6}\delta + \frac{16\tilde{D}_{11}}{3\lambda^2}(\delta - \delta_c) \qquad (23)$$

The predicted load-deflection response in Stage III is indicated by the dashed line in Fig. 2. Because the back facesheet failure load was overpredicted only a small portion of this graph is actually used in the predicted response. The load drop at E corresponds to tensile failure of the front facesheet.

5 Low-Velocity Impact Response

The impact response of the panel is found from the two degree-of-freedom mass-spring-dashpot system shown in Fig. 4. The projectile mass is denoted M_o, and the effective mass of the top facesheet and sandwich are represented by m_f and m_s, respectively. Expressions for the effective facesheet and sandwich masses are derived by assuming the local and global velocities are distributed the same as their deformations. The local deformation and global deformation are given by $\delta = X_1 - X_2$ and $\Delta = X_2$, respectively. The local indentation resistance P_l and the global spring stiffness K_g are found from quasi-static results and adjusted with the strain rate-dependent material properties of the facesheet and core. High strain material tests show that the stiffness and strength of the E-glass/vinyl ester increases with increasing strain rate [11]. High strain rate tests on polymeric foams indicate that they are fairly rate insensitive [12]. The Coremat material properties are therefore assumed to be the same as in quasi-static tests. In addition to the local and global stiffness, a linear dashpot is used to represent damping of the Coremat. The damping constant for the dashpot is calculated from the impact test results since there is no published data on Coremat damping properties.

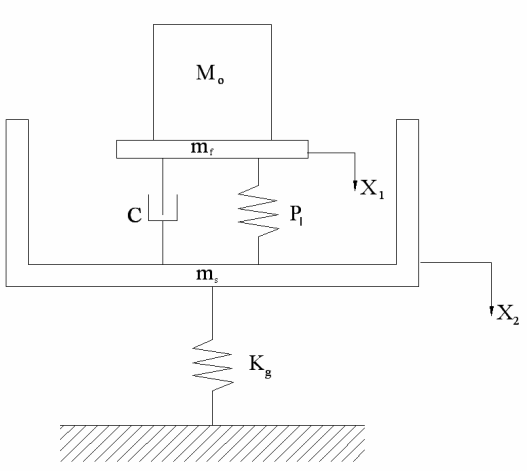

Fig. 4 Two degree-of-freedom model for impact of composite sandwich panel.

The equations of motion for the two-degree-of-freedom system are

$$(M_o + m_f)\ddot{X}_1 + P_l + c(\dot{X}_1 - \dot{X}_2) = 0 \qquad (24)$$

and

$$m_s\ddot{X}_2 - P_l - c(\dot{X}_1 - \dot{X}_2) + K_g X_2 = 0 \qquad (25)$$

The initial conditions for the two-degree-of-freedom system are as follows: $X_1(0) = 0$, $X_2(0) = 0$, $\dot{X}_1(0) = V_o$, and $\dot{X}_2(0) = 0$, where V_o is the initial velocity of the projectile.

Equations (24) and (25) represent a nonlinear, coupled initial-value problem. An ode solver was used in MATLAB to solve for X_1 and X_2. The contact force between the projectile and the impacted facesheet is given by

$$F = -M_o\ddot{X}_1 \qquad (26)$$

Each failure event occurring during transient deformation would decrease the kinetic energy of the system. The energy absorbed by delamination/debonding is the product of the interlaminar shear fracture toughness and appropriate areas. These areas may be estimated from Eq. (15) and the delamination and debonding

loads. The core shear fracture energy is given also given by the product of the core transverse shear fracture toughness and its associated fracture area. The fracture energy due to petaling of the back and front facesheets are estimated from the tear energy of the E-glass/vinyl ester. Expressions for the tear energy associated with petaling are taken from Lin and Hoo Fatt [5].

Figure 5 compares the calculated contact force with test data for panels impacted by a 10 kg projectile and exhibiting neither top or bottom facesheet fracture. A 10% increase in the facesheet stiffness and strength is assumed and the damping constant is estimated at 159.8 Ns/m. The analytical model is able to predict an average contact force to within 10% of the experimental data. In all of these tests, the maximum global deformations were less than 36.8 mm, which is about the deflection at which the back facesheet would have failed. It is assumed both the stiffness and strength of the facehseet would increase with increasing strain rate by the same amount such that the global deflection at back facesheet failure remains the same in the impact tests.

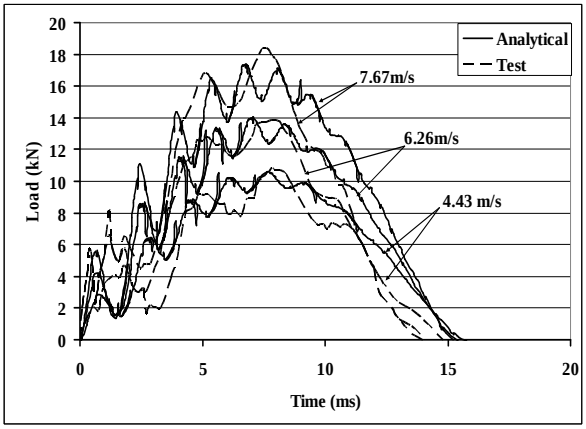

Fig. 5 Contact force history of impact with 10 kg mass projectile at 4.43, 6.26 and 7.67 m/s.

Core shear fracture, delamination and debonding energy should be subtracted from the kinetic energy of the system at the instant they occur. The time duration of these events are instantaneous compared to the sandwich response time since these failures constituted brittle or unstable crack propagation. The energy associated with delamination and debonding is very small and has negligible effect on the solution. The core transverse shear fracture energy could not be estimated for lack of data on the core transverse fracture toughness. It is assumed to be negligibly small, although it was noticed that there was a load drop in the test data at about the load core shear fracture would occur.

With increasing mass or projectile velocity, damage would occur. Figure 6 compares the calculated and experimental contact forces for the panel with an impact mass of 20 and 30 kg and an impact velocity of 6.26 m/s.

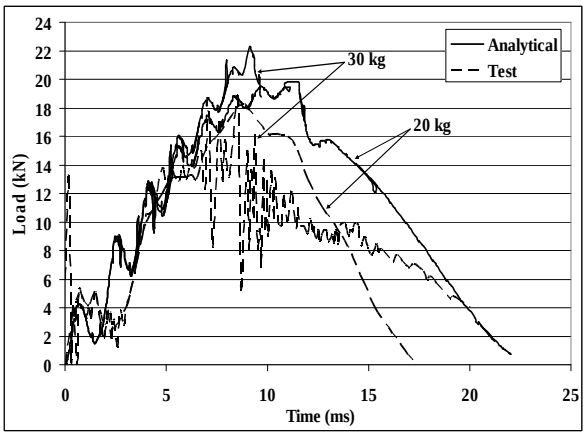

Fig. 6 Contact force history of impact with 20 and 30 kg mass projectile at 6.26 m/s.

Impact with the 20 kg just causes fracture of the back facesheet when the contact force is at a maximum value. At this time, the global panel deflection is almost 36.8 mm. The final deflections and velocities at this time are used as initial conditions in a new simulation of the coupled equations of motion with the Stage III local-indentation response instead of the Stage I/II local-indentation response. The damping constant is assumed to increase to 1000 Ns/m since damping associated with localized core shearing is higher than damping associated with core crushing. The predicted solution is very close to the test data in Stage I/II, but the contact force in Stage III is about 20% higher than the test results. This is because loss of kinetic energy due to tearing of the back facesheet is not accounted for since the velocities at the instant of back facesheet fracture are zero at the peak contact force.

Impact with the 30 kg mass causes complete panel perforation. Unlike the 20 kg mass impact, back facesheet failure takes place at 8.1 ms, about

4.4 ms before the time peak contact force would have occurred. The tear energy is subtracted from the kinetic energy of the back facesheet at this time and a new residual velocity of the back facesheet is calculated. The coupled equations of motion are then solved again using this residual velocity and the corresponding displacements and projectile velocity as initial conditions, the Stage III local indentation response and the damping constant set to 1000 Ns/m. Immediately the local deflection $X_1 - X_2$, exceeds the amount to cause front facesheet failure. Therefore both back and front facesheet take place at the same time. This predicted result is similar to what was found in the test.

6 Conclusions

Analytical models were derived for quasi-static and impact perforation of an E-glass/vinyl ester and Coremat sandwich panel. The panel deformation was decomposed into local indentation and global deformation. An equivalent two degree-of-freedom mass-spring-dashpot system was used to find the dynamic response of the composite sandwich panel subjected to a drop-weight impact by a rigid hemispherical-nose projectile. Equivalent spring resistances were derived from the quasi-static load-displacement response and adjusted dynamic material properties of the facesheet. Several failure modes were considered, including delamination, debonding, core shear fracture, and top and bottom facesheet failures.

Analytical predictions of the quasi-static load-deflection response were within 5% of the test data. However, the calculated failure load was about 25% higher than the test data. This type of accuracy is typical of using the minimum potential energy to approximate the load-deformation response of panels. Analytical predictions of the dynamic response, in particular the contact force history, also compared very well with the test data. The two degree-of-freedom model was able to simulate the correct physics of impact perforation. Without failure of either back or front facesheets, predicted contact force histories were within 10% of test data.

Acknowledgement

The authors acknowledge financial support from Dr. Yapa Rajapakse at the Office of Naval Research under grant N00014-07-1-0423. The authors would like to thank Dr. R. A. W. Mines for providing experimental results on the static and low-velocity perforation of the E-glass/vinyl ester and Coremat sandwich panel.

References

[1] Belingardi G., Cavatorta M.P., Duella R. "Material characterization of a composite-foam sandwich for front structure of a high speed train," *Composite Structures*, Vol. 61, No. 1, pp. 13-25, 2003.

[2] Wen H.W., Reddy T.Y., Reid S.R., Soden P.D. "Indentation, penetration and perforation of composite laminates and sandwich panels under quasi-static and projectile loading," *Key Engineering Materials*, Vols. 141-143, pp. 501-552, 1998.

[3] Mines R.A.W., Worrall C.M., Gibson A. G. "Low velocity perforation behavior of polymer composite sandwich panels," *International. Journal of Impact Engineering*, Vol. 21, No. 10, pp. 855-879, 1998.

[4] Lantor, B.V. "Firet Coremat data sheet," Veenendaal, The Netherlands, 1993.

[5] Lin C., Hoo Fatt, M.S. "Perforation of sandwich panels with honeycomb cores by hemispherical-nose projectiles," *Journal of Sandwich Structures and Materials*, Vol. 7, No. 2, pp. 113-172, 2005.

[6] Mines R.A.W., Jones N. "Approximate elastic-plastic analysis of the static and impact behavior of polymer composite sandwich beams," *Composites*, Vol. 26, No. 12, pp. 803-814, 1995.

[7] Stevanovic D., Jar P.-Y.B., Kalynasundaram S., Lowe A. "On crack-Initiation conditions for mode I and mode II delamination testing of composite materials," Composite *Science and. Technology*. Vol. 60, No. 9, pp. 1879-1887, 2000.

[8] Kolat K., Neser G.., Ozes C. "The effect of sea water exposure on the interfacial fracture of some sandwich systems in marine use," *Composite Structures*, Vol. 78, No. 1, pp. 11-17, 2007.

[9] Olsson R., Donadon M.V., Falzon B.G. "Delamination threshold load for dynamic impact on plates," *Int J Solids Struct*, Vol. 43, No. 10, pp. 3124-3141, 2006.

[10] Swaminathan G., Shivakumar K.N., Sharpe M. "Materials property characterization of glass and carbon/vinyl ester composites." *Composite Science and Technology*, Vol. 66, No. 10, pp. 1399-1408, 2006.

[11] Johnson H.E., Louca L.A., Mouring S.E. "Current research into modelling of shock damage to large scale composite panels." *J. Mater. Sci*., Vol. 41, No. 20, pp 6655-6672, 2006.

[12] Ouellet S., Cronin D., Worswick M. "Compressive response of polymeric foams under quasi-static, medium and high strain rate conditions," *Polymer Testing*, Vol. 25, No. 6, pp. 731-741, 2006.